A New Approach for Classification of Human Gait Based on Time-Frequency Feature Representations

Irena Orović, Srdjan Stanković, Moeness Amin

***Abstract*— We introduce a new and simple technique for human gait classification based on the time-frequency analysis of radar data. The focus is on the classification of arm movements to discern free vs. confined arm swinging motion. The latter may arise in hostage situation or may be indicative to carrying objects with one or both hands. The motion signatures corresponding to the arm and leg movements are both extracted from the time-frequency representation of the micro-Doppler. The time-frequency analysis is performed using the multiwindow S-method. With the Hermite functions acting as multiwindows, it is shown that the Hermite S-method provides an efficient representation of the complex Doppler associated with human walking. The proposed human gait classification technique utilizes the arm positive and negative Doppler frequencies and their relative time of occurrence. It is tested on various real radar signals and shown to provide an accurate classification.**

***Index Terms*— Time-frequency distributions, radar signals, human walking, micro-Doppler signatures**

I. Introduction

Among several possible technologies, including acoustics, thermal, optical, and radio frequency, RF based technology is considered an attractive modality for human motion detection and classifications, as it can be applied under all weather, light, smoke, and for targets obstructed by opaque material. Recently, radar has been successfully used in urban sensing applications and through wall imaging [1]-[5].

This paper considers radars for the classification of human gait based on distinctions in the walking person's arm movements. In particular three types of walking motions are of interest: 1) Free arm-motion (FAM) characterized by swinging of both arms, 2) Partial arm-motion (PAM) which corresponds to a motion of only one arm, and 3) No arm-motion (NAM) which corresponds to no motion of either arm. The NAM is referred to as a stroller or saunterer [6]. The last two classes are commonly associated with a person walking with his/her hand(s) in the trouser pockets or a person carrying light small or large heavy objects, respectively. All three categories are considered important in law enforcement and homeland security operations.

The radar micro-Doppler for human gait has been an active area of research for the last decade [7], [8]. In addition to the main Doppler shift due to the motion of the human torso, the relative motions of the limbs to the body introduce micro-Doppler which presents itself as a time-varying frequency shift. The complex nonstationary Doppler signature of human walking can be revealed via a joint time-frequency signal representation in lieu of the traditional Fourier transform, of the radar return. The degree of clarity and depiction of the time-dependent Doppler frequency for each part of the human body in motion can vary depending on the time-frequency analysis tool employed. Compared to other methods, time-frequency distributions, which capture the instantaneous frequency laws are most suitable for the underlying application [9]-[13].

Classifications of the above types of human gait were considered in [6], [14]-[16]. The work in [6] only dealt with FAM and NAM types and used Spectrogram for the distribution of Doppler signal power in the time-frequency domain. This work, though important, did not consider distinctions in the types of motion, but rather estimated the human walking parameters by minimizing the difference between simulated Thalmann model [16] and real measurements. Human gait classifications of the three types FAM, PAM, and NAM, were discussed in [14] based on subspace learning using principal component analysis (PCA). The training set consists of feature vectors defined as either time or frequency snapshots taken from the spectrogram of radar backscatter. This method, although generated promising classification results, is nonparametric and did not explicitly utilize the periodic and evolving nature of the human gait in the three motion types. The time-frequency classifier in [15] applied distance measures between training and test sets represented by the time-frequency distributions of the corresponding Doppler signals. This classifier is also a nonparametric method. It neither selects nor does it separate the key and distinctive Doppler features, associated with the arms' motions. The classifier employed in [17] was based on SVM and considered several types of human motions,

Manuscript received January 20, 2010.

I. Orović and S. Stanković are with the Electrical Engineering Department, University of Montenegro, 81000 Podgorica, Montenegro.

M. Amin is with the Center for Advanced Communications, Villanova University, Villanova, PA 19085 USA

The corresponding author is Irena Orović, phone: +38267516795, fax: +382 20 242 667, E-mail: irenao@ac.me.

including running and crawling. It is a parametric technique and used different numerical features of the human motion. This technique, however, did not consider the classification of the above three classes and their corresponding salient feature.

Our contribution to the above gait classification problem is twofold. We apply the recently introduced multiwindow S-method [18] as a high time-frequency concentration technique, in lieu of Wigner distribution, spectrograms, or other time-frequency signal representations. It is shown that this method, applied to the three types of human gait, effectively reveals the arm motions in the time-frequency domain. The result of the multiwindow S-method is used to provide the perimeter of the arm motions. A simple classification technique is then employed which acts on the arm perimeters and incorporates the positive and negative strides of the arm swings as well as their relative time of occurrences. In this respect, the proposed method does not predicate on learning or reference sets, as in the case in both [14], [15] and, as such, avoids the potential mismatch between learning and test sets which is likely responsible for the rather high classification errors exhibited in applying those methods. It is noted that the multiple windows are obtained by using the Hermite functions, which have good time-frequency localization property [19], [20]. By employing only a few Hermite functions (of lowest orders), the complexity of realization is slightly increased comparing to the standard S-method.

The paper is organized as follows. Section II provides the theoretical background on the time-frequency analysis. A brief mathematical model of Micro-Doppler phenomenon induced by human motion is given in Section III.A, while the time-frequency based classification procedure is proposed in Section III.B. The application of the proposed procedure is demonstrated through the examples with real radar signals in Section IV. This Section also contains a performance comparison between the Hermite S-method and both the spectrograms and S-method applied alone without the multiwindowing. The concluding remarks are given in Section V.

II. Theoretical Background- Time-Frequency Analysis

The time-frequency representation of a signal $s(t)=Ae^{j\phi(t)}$ that provides the energy distribution along the instantaneous frequency may be written as [21]:

$$TFR(t,\omega)=2\pi A^2\delta(\omega-\phi'(t))*_\omega FT\left\{e^{jQ(t,\tau)}\right\}*_\omega W(\omega), \quad (1)$$

where $Q(t,\tau)$ is a spread factor defining the distribution spread around the instantaneous frequency, the Fourier transform is denoted by FT, while $W(\omega)$ is the Fourier transform of a window in time domain. The simplest time-frequency representation is obtained by using the short-time Fourier transform (STFT):

$$STFT(t,\omega)=\int_{-\infty}^{\infty} s(t+\tau)w(\tau)e^{-j\omega\tau}d\tau, \quad (2)$$

where $w(\tau)$ is a window function. The energetic version of the *STFT* is called spectrogram, and it is the squared module of the STFT: $SPEC(t,\omega)=|STFT(t,\omega)|^2$. The spectrogram can be successfully used in many applications. However, there is always a trade off between time and frequency resolution. Also, the spread factor contains all higher phase derivatives:

$$Q(t,\tau)=\phi^{(2)}(t)\frac{\tau^2}{2!}+\phi^{(3)}(t)\frac{\tau^3}{3!}+\phi^{(4)}(t)\frac{\tau^4}{4!}+... \quad (3)$$

The resolution in the time-frequency domain is improved by introducing quadratic time-frequency distributions, such as the Wigner distribution.

$$WD(t,\omega)=\int_{-\infty}^{\infty} w\left(\frac{\tau}{2}\right)w^*\left(-\frac{\tau}{2}\right)s\left(t+\frac{\tau}{2}\right)s^*\left(t-\frac{\tau}{2}\right)e^{-j\omega\tau}d\tau\,. \quad (4)$$

Note that, in the case of the Wigner distribution, the even phase derivatives disappear from the spread factor:

$$Q(t,\tau)=\phi^{(3)}(t)\frac{\tau^3}{2^2 3!}+\phi^{(5)}(t)\frac{\tau^5}{2^4 5!}+\phi^{(7)}(t)\frac{\tau^7}{2^6 7!}+... \quad (5)$$

The S-method is defined as a quadratic distribution that combines good properties of the spectrogram and the Wigner distribution [22]. It preserves the auto-terms concentration as in the Wigner distribution and additionally reduces the noise influence [23] (the spread factor is also given by (5)). Furthermore, the S-method can be implemented in a numerically very efficient way, which makes it attractive for applications. It is given by:

$$SM(t,\omega)=\int_\theta P(\theta)STFT(t,\omega+\theta)STFT^*(t,\omega-\theta)d\theta, \quad (6)$$

where $P(\theta)$ is the frequency domain window of finite length. The convergence within $P(\theta)$ is very fast, providing high auto-terms concentration with only a few convolution terms. At the same time, it reduces (or removes) the cross-terms in the Wigner distribution [22].

Additional concentration improvement for time-varying spectrum has been achieved by introducing multiwindow time-frequency analysis [23]-[26]. Because of their orthogonality and attractive localization properties [26], the Hermite functions can be used as optimal windows. The k-th function is recursively calculated as:

$$\Psi_k(t)=t\sqrt{\frac{2}{k}}\Psi_{k-1}(t)-\sqrt{\frac{k-1}{k}}\Psi_{k-2}(t), \quad "k\geq 2, \quad (7)$$

where $\Psi_0(t)=\frac{1}{\sqrt[4]{\pi}}e^{-t^2/2}$, $\Psi_1(t)=\frac{\sqrt{2}t}{\sqrt[4]{\pi}}e^{-t^2/2}$.

The multiple windows have been initially used for the multiwindow spectrogram, given by [23]-[26]:

$$MSPEC(t,w)=\frac{1}{2\pi}\sum_{k=0}^{K-1}d_k(t)\left|\int s(t)\Psi_k(t-t)e^{-jwt}dt\right|^2, \quad (8)$$

where d_k are the weighting coefficients, and K is the number of employed Hermite functions. The weighting coefficients are obtained by solving the system:

$$\sum_{k=0}^{K-1} d_k(t) \frac{\int A^2(t+\tau)\Psi_k^2(\tau)\tau^n d\tau}{\int A^2(t+\tau)\Psi_k^2(\tau)d\tau} = \begin{cases} 1 & \text{for } n=0 \\ 0 & \text{for } n>0 \end{cases}.$$

All higher phase derivatives up to $(K+1)^{\text{th}}$ are removed from the spread factor, which is given in the form:

$$Q(t,\tau)=\phi^{(K+1)}(t)\frac{\tau^{K+1}}{(K+1)!}+\phi^{(K+2)}(t)\frac{\tau^{K+2}}{(K+2)!}+\phi^{(K+3)}(t)\frac{\tau^{K+3}}{(K+3)!}+... \quad (9)$$

Similarly, a multiwindow version of the standard S-method, i.e. the Hermite S-method, has been introduced as a convolution of Hermite based STFTs [18]:

$$MSM(t,w)=\sum_{k=0}^{K-1}\int_{\theta} P(\theta)d_k(t)STFT_k(t,w+\theta)STFT_k^*(t,w-\theta)d\theta, \quad (10)$$

where $STFT_k(t,w)$ is the STFT calculated by using the k-th order Hermite function $\Psi_k(t)$. The spread factor for multiwindow S-method contains only half of the terms that exists within the spread factor of the multiwindow spectrogram.

Although the multiwindow approach has been derived by using the concept of conditional mean frequency, it can be used for radar signals considered in this paper. Namely, the experiments show that the multiwindow S-method may additionally reduce the inner-interferences and noise, and thus, with only a few window functions it produces slightly better representation than the standard S-method.

III. Application of the Time-Frequency Analysis in Human Walking Characterization

Here, we consider the problem of signatures extraction that would allow one to distinguish between the three different types of human gait described in the Introduction, namely the FAM, PAM, and NAM. We, therefore, focus on radar signal components corresponding to the arms swinging. We assume that the arm motion is pronounced in the human walking which means that the person has a full swing of the arm when it is in motion. We also assume that the motion is regular and homogenous, in the sense that for FAM, the two arms are moving approximately in the same manner. It means that both arms pass by the body (through the *P* points in Fig 1), in opposite directions, approximately in the same moment (the time difference Δt is small). The same holds for the points (*M* in Fig 1) where the arms reach the maximum in both directions.

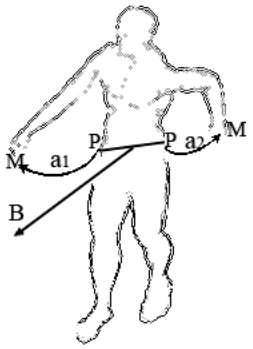

Fig. 1. Main motion – B, swinging arms A1 and A2

A. Basic mathematical description of Micro-Doppler phenomenon induced by the human motion

In the coherent radar applications, the signal is returned from the target with a phase change due to the variations in range. Different body parts are moving with different velocities and thus, produce different shifts. The signal returned from the swinging arms may include frequency modulation that will produce the sidebands around the body Doppler. The received Doppler can be modeled as follows [27]:

$$s(t) = Ae^{j(2\pi f_0 t+\phi(t)),} \quad (11)$$

where A is the reflectivity of the chosen reflecting point, f_0 is the carrier frequency of the transmitted signal, while $\phi(t)$ is the time-varying phase change. For an oscillating/vibrating object,

$$\phi(t) = \frac{4\pi D_v}{\lambda}\sin(\omega_v t). \quad (12)$$

The parameter D_v represents the amplitude of vibration, or maximum deviation from the center of the motion, and λ is the wavelength of the transmitted signal. The corresponding induced micro-Doppler frequency is the derivative of the phase and is given by:

$$f_D(t) = \frac{1}{2\pi}\frac{d\phi(t)}{dt} = \frac{1}{2\pi}\frac{2}{\lambda}D_v\omega_v\cos(\omega_v t). \quad (13)$$

Hence, in this case, micro-Doppler represents the sinusoidal function of time at the frequency ω_v.

B. The classification procedure for real radar signals based on the time-frequency analysis

A features extraction scheme is proposed. It does not measure distances as in [6], [15], neither does it apply any subspace projection as in [14]. As such, the proposed scheme avoids the construction of learning or reference sets, as in [17], which could be behind the undesired classification performance by these methods. Our method, in essence, recognizes that the time-frequency representation exhibits some symmetry or anti-symmetry for each type of arms swinging. The features extracted are based on the envelopes

or the perimeters of the arms depicted in the time-frequency domain which is generated using the Hermite S-method. The use of the envelops bears similarity to the SVM method proposed in [17]. The difference is in the features underlying these envelopes and the way it is used and processed by the classifier.

In the first step of this procedure, the strongest components corresponding to the main motion (torso and legs motion), will be removed. It is obtained by using time-frequency based support function defined as:

$$S_1(t,\omega)=\begin{cases}0, & for \quad (t,B(t)-\delta)<(t,\omega)<(t,B(t)+\delta)\\ 1, & elsewhere,\end{cases} \tag{14}$$

where the width of main motion region along frequency axis is $2\delta+1$, and

$$B(t)=\arg\left\{\max_{\omega}\left|MSM(t,\omega)\right|\right\}. \tag{15}$$

Here it is assumed that the maximal value is centered, which might not be always true. However, even the rough approximation of the main motion region is sufficient, since the aim is just to remove the relative strong components in order to highlight the weaker arms movements. An illustration of the region that will be removed by the support function $S_1(t,\omega)$ is given in Fig 2.

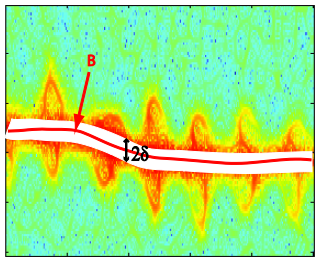

Fig 2. An illustration of the region corresponding to the main motion

In order to reduce the influence from other moving parts (apart from arms), the additional support function is defined as:

$$S_2(t,\omega)=\begin{cases}1, & for \quad (t,\omega):\xi<\left|MSM(t,\omega)\right|<Thr\\ 0, & elsewhere,\end{cases} \tag{16}$$

where Thr is an energy floor, while ξ is used to remove small noise outside the region with signal components. Finally, $S_1(t,\omega)$ and $S_2(t,\omega)$ are combined to obtain the resulting support function:

$$S(t,\omega)=S_1(t,\omega)\cap S_2(t,\omega). \tag{17}$$

The points within $S(t,\omega)$ could be divided into two sets: positive frequency points and negative frequency points, respectively, above and below the main trajectory (torso motion component). If arms are swinging during walking, these sets of points describe the envelopes of the swinging motion. However, since they are noisy data sets, some additional processing is required in order to expose their features. Thus, a curve smoothing procedure is applied on both data sets. This procedure can be observed as a nonparametric local fit that can be done by filtering (averaging) or local regression. The smoothness is controlled by the span ψ, i.e., by the window width used in the smoothing procedure. Here, the procedure based on the moving average filter is used and smooth curves i.e., modeling functions, are obtained:

$$\Phi\left\{S(t,\omega)\right\}\xrightarrow{\omega>B(t)}f_1(t), \tag{18}$$

$$\Phi\left\{S(t,\omega)\right\}\xrightarrow{\omega<B(t)}f_2(t).$$

Note that the parametric modeling can be used, as well. For example, Gaussian type of fit (up to the seventh order: $a_1\exp(-((x-b_1)/c_1)^2)+...+\ a_7\exp(-((x-b_7)/c_7)^2)$ provides very similar results.

The modeling functions for walking with both arms swinging (FAM) and walking without arms swinging (PAM) are illustrated in Fig 3 and Fig 4, respectively.

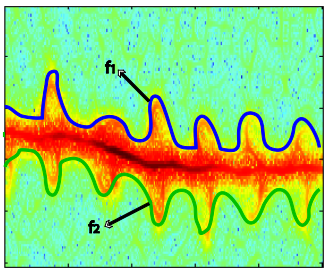

Fig. 3. Modeling functions f_1 and f_2

Let us first consider the following two hypotheses: h_1 – (NAM), h_2 – (PAM, FAM). The functions f_1 and f_2 could be generally written as:

$$\begin{aligned}f_1(t)&=B(t)+\delta\pm\xi_{f1}(t),\\ f_2(t)&=B(t)-\delta\pm\xi_{f2}(t),\end{aligned} \tag{19}$$

where δ is a constant defined in (14) to approximate the main motion width (2δ+1) along frequency axis, while $\xi_{f1}(t)$ and $\xi_{f2}(t)$ represent variations with respect to the main motion. Note that, $\xi_{f1}(t)$ and $\xi_{f2}(t)$ are mainly the consequence of arms swinging. Otherwise, if no arm swinging is present, the variations may appear due to the noise or some legs' movements, and they are quite lower than in the case of arms swinging. An illustration is given in Fig 4. Thus, a decision rule can be defined as:

$$MSE=MSE_1+MSE_2=\frac{1}{T}\sum_t\xi_{f1}^2(t)+\frac{1}{T}\sum_t\xi_{f2}^2(t)\ \begin{matrix}h_2\\ \geq\\ <\\ h_1\end{matrix}\ \xi_{Thr}, \tag{20}$$

where MSE is the total mean square error, while ξ_{Thr} is a predefined value of the mean square error. If h_2 is true, then the two additional hypotheses are considered: h_{21} – one arm

swinging (PAM), h_{22} – both arms swinging (FAM). If h_{22} is true, the curves $f_1(t)$ and $f_2(t)$ look "symmetrical" across the walking trajectory $B(t)$. Here, the "symmetrical" behavior is described as follows: each local maximum on f_1 has a corresponding local minimum on f_2 which is located in time vicinity Δt.

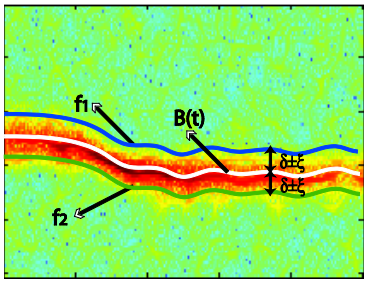

Fig 4. Signal with no arms movements: f_1 and f_2 should be on a distance δ from $B(t)$ with small variations ξ_{f1} and ξ_{f2}, respectively

Otherwise, the functions $f_1(t)$ and $f_2(t)$ are "asymmetrical" and the hypothesis h_{21} is true. This classification rule can be written as:

$$arg\{l\max(f_1(t))\} - arg\{l\min(f_2(t))\} \underset{h21}{\overset{h22}{\lessgtr}} \Delta t_T, \qquad (21)$$

where $l\max(f_1(t))$ represents the local maximum of $f_1(t)$, $l\min(f_2(t))$ is a local minimum of $f_2(t)$, while Δt_T is a threshold value for Δt.

IV. Examples

Example 1: In this Section, the proposed classification scheme is tested on the set of real data collected at the Radar Imaging Lab, Center for Advanced Communications, Villanova University. The experiments were performed with the radar operating at a carrier frequency 2.4 GHz, with a transmit power level 5 dBm. The instantaneous frequency bandwidth is 70 kHz. The sampling frequency of the original signals is 1 kHz. For the calculation of the Hermite S-method, the signals are further downsampled by factor of 4.

The radar data are collected from different human targets. Also, the data were collected at angles 0 and 30 degrees with respect to the radar's line-of-sight. Three types of human motions were considered: NAM, i.e., walking with no arm swinging, PAM, i.e., walking with one arm swinging, and FAM, i.e., walking with both arms swinging.

For all tested signals, the Hermite S-method is calculated by using three Hermite functions of the lowest order: k=0,1,2, with 512 samples within the windows. The parameter L=3 is used to define the width of frequency window $P(l)$. Furthermore, the value of parameter δ=6 (approximately 1.5Hz) is used to approximate the width of signal components representing the main motion. The same value is used for all tested signals. The approximation of the main motion width could be further considered in some future work.

The energy floor Thr within $S_2(t,\omega)$ is obtained experimentally and it is set to the value $2\cdot10^{-4}$ for all tested signals. The implementation of the proposed procedure is performed by using Matlab 7. The smooth curves f_1 and f_2 are obtained by applying the moving average method with smoothing span ψ=45.

In order to distinguish human walking with and without arms, the mean square errors (MSE) are calculated according to (20). The results are presented in Table I. The significantly lower MSEs are obtained for signals that do not contain arms swinging. Thus, according to the results for the considered set of signals $\xi_{Thr} = 20$ can be used for classification.

TABLE I. MSEs obtained for tested signals without arms movements (NAM) and signals with arms movements (PAM and FAM)

No arms (NAM)		One or both arms (PAM or FAM)	
Signals	**MSE**	**Signals**	**MSE**
Sig 1	5.1	**Sig 9 (1 arm)**	69.7
Sig 2	4.2	**Sig 10 (2 arms)**	57.5
Sig 3	16.6	**Sig 11 (1 arm)**	211
Sig 4	13.6	**Sig 12 (2 arms)**	127.8
Sig 5	13.4	**Sig 13 (2 arms)**	146.4
Sig 6	10.3	**Sig 14 (1 arm)**	112
Sig 7	5.9	**Sig 15 (1 arm)**	83.3
Sig 8	3.2	**Sig 16 (2 arms)**	46.5

The classification between one arm (PAM) and both arms swinging (FAM) is now considered. The results for these types of signals are illustrated in Fig 5 and Fig 6. The Hermite S-method of signal containing both arms swinging is shown in Fig 5.a. The time-frequency signatures, used in the classification process are illustrated in Fig 5.b, while the corresponding support function is given in Fig 5.c. The curves f_1 and f_2 are given in Fig 5.d. Note that in these experiments, the time distance Δt between the local maximum on f_1 and corresponding minimum on f_2 is around 20 samples. On the other hand, in the case of walking with one arm swinging, Δt is higher, since both maximum on f_1 and minimum on f_2 are from the same arm swinging. The Hermite S-method, time-frequency signatures and corresponding support function, for walking with one arm swinging, are illustrated in Fig 6.a to Fig 6.c, respectively. The functions f_1 and f_2 are illustrated in Fig 6.d. It can be observed that Δt is significantly higher than 20 samples (between 100 and 200 samples for the considered signal). The minimal and maximal values of Δt are given in Table II. Note that there is a significant gap between the values of Δt for one and two arms swinging. The threshold value Δt_T could be set between the lowest **min(** Δt **)** for one arm swinging (Signal 5, value 109, in Table II) and highest **max(** Δt **)** for both arms swinging (Signal 4, value 25, in

Table II). Thus, $\Delta t_T = 67$ can be used. Also, the mean values m and standard deviations σ, for min(Δt) and max(Δt) are given in Table III.

For each of the two classification procedures the probability of error is calculated as follows:

$$Perr = \int_{T}^{\infty} p_1 P_1(\lambda) d\lambda + \int_{-\infty}^{T} p_2 P_2(\lambda) d\lambda = \frac{1}{4} erfc\left(\frac{T-\mu_1}{\sqrt{2}\sigma_1}\right) + \frac{1}{2} - \frac{1}{4} erfc\left(\frac{T-\mu_2}{\sqrt{2}\sigma_2}\right),$$

where p_1=p_2=1/2 and the normal distribution is assumed for P_1 and P_2. The mean values and standard deviations of classification parameters (MSE for the first and Δt for the second classification) are denoted as μ and σ, respectively. They are calculated from the values obtained in the experiments. The parameter T is threshold, which is equal to ξ_{Thr} for the first and Δt_T for the second procedure. The results are shown in Table IV.

TABLE II. MINIMAL AND MAXIMAL VALUES OF Δt FOR A SET OF TESTED SIGNALS

	Angle	min(Δt) in samples	max(Δt) in samples	No of arms
Signal 1	30	19	22	2
Signal 2	0	0	20	2
Signal 3	0	2	22	2
Signal 4	0	5	25	2
Signal 5	30	7	20	2
Signal 6	0	2	27	2
Signal 7	30	109	140	1
Signal 8	0	100	160	1
Signal 9	30	120	200	1
Signal 10	0	115	140	1
Signal 11	0	125	140	1
Signal 12	30	140	150	1

TABLE III. MEAN VALUES AND STANDARD DEVIATIONS OF MINIMAL AND MAXIMAL Δt

No of arms	2 arms	1 arm
m{min(Δt)} **in samples**	5.83	118.16
σ{min(Δt)} **in samples**	6.91	13.79
m{max(Δt)} **in samples**	22.66	155
σ{max(Δt)} **in samples**	2.8	23.45

TABLE IV. PROBABILITIES OF ERROR FOR THE TWO CLASSIFICATION PROCEDURES

Classification between NAM and PAM/FAM					
Classification parameter MSE				**Threshold T**	**Total probability of error**
MSE{NAM}		**MSE{PAM or FAM}**			
μ_1	σ_1	μ_2	σ_2		
9.037	5.091	106.77	54.62	T=ξ_{Thr}=20	**P_{err}=3.54%**

Classification between PAM and FAM					
Classification parameter Δt				**Threshold T**	**Total probability of error**
Δt {FAM-2 arm}		**Δt {PAM-1 arm}**			
μ_1	σ_1	μ_2	Σ_2		
14.25	10.12	136.58	26.57	T=Δt_T=67	**P_{err}=0.22%**

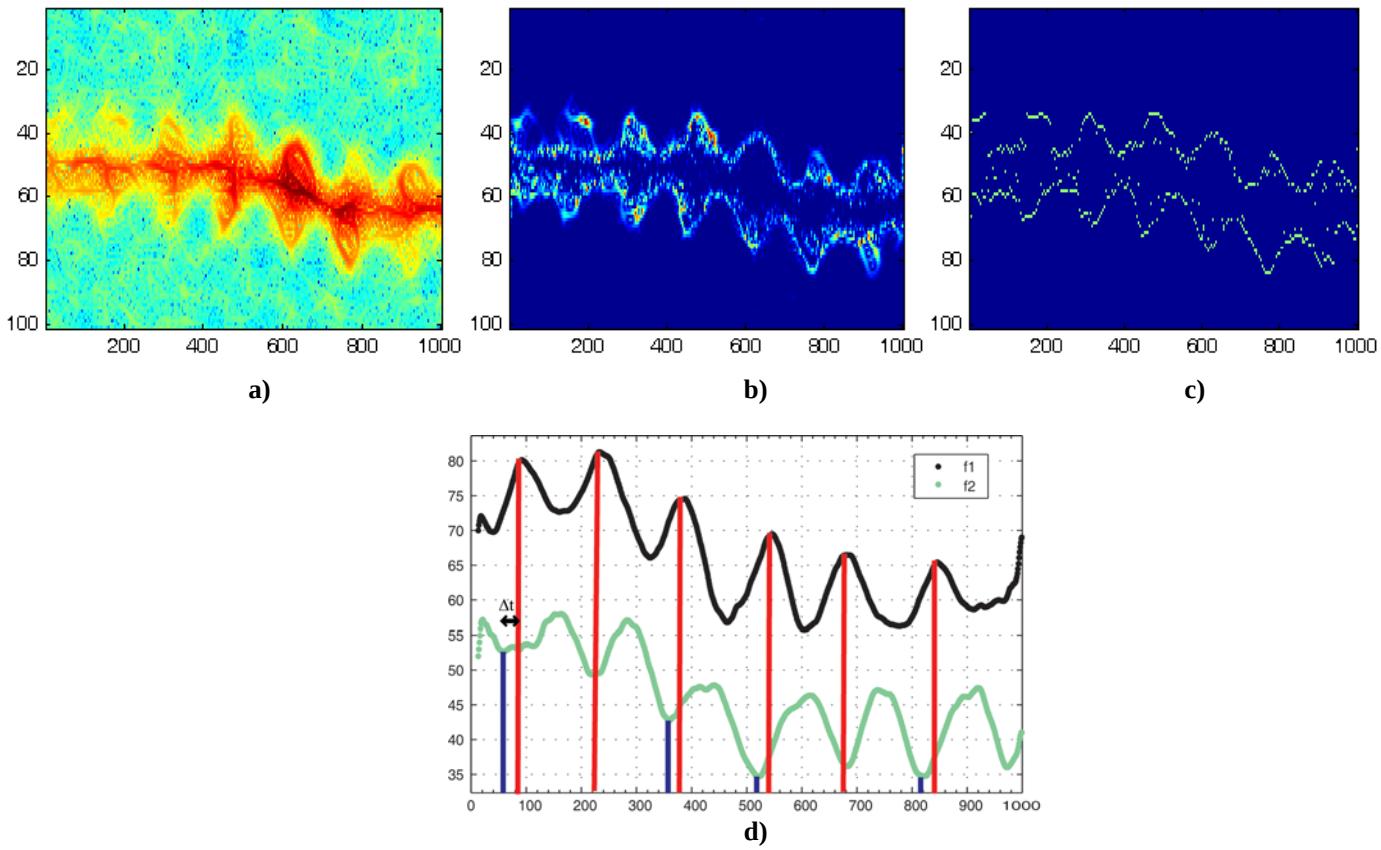

Fig 5. Both arms swinging: a) Hermite S-method, b) time-frequency signatures, c) support function, d) functions f_1 and f_2

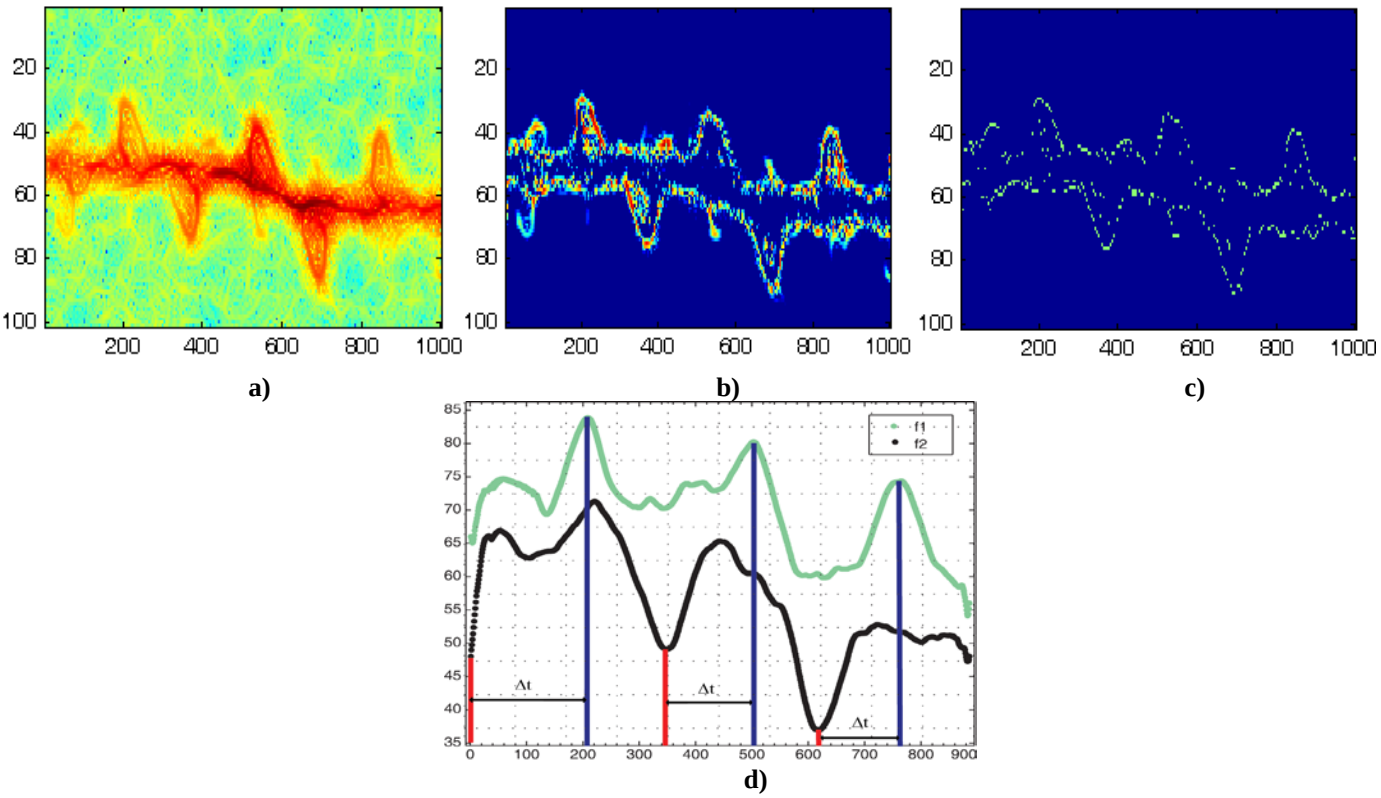

Fig 6. One arm swinging: a) Hermite S-method, b) time-frequency signatures, c) support function, d) functions f_1 and f_2

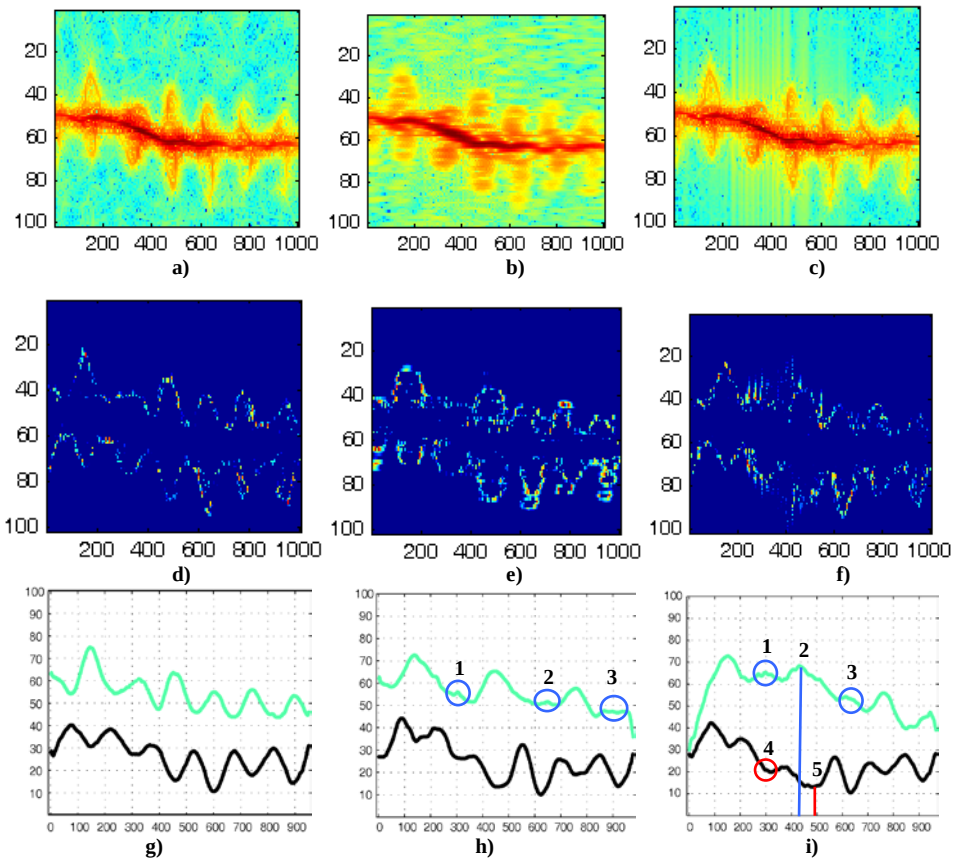

Fig 7. A comparison of different time-frequency distributions: a) Hermite S-method, b) Spectrogram, c) S-method; Time-frequency signatures obtained by using: d) Hermite S-method, e) Spectrogram, f) S-method; Modeling functions based on the: g) Hermite S-method, h) Spectrogram, i) S-method

Example 2: The advantage of the Hermite S-method over the spectrogram and the standard S-method, for the considered application, is illustrated in this example.

The noisy radar signal is considered (white Gaussian noise is added), with SNR≈25dB. The considered signal describes walking with both arms swinging. The Hermite S-method, the spectrogram and the standard S-method are given in Fig 7.a-c, respectively. The corresponding time-frequency signatures are plotted in Fig 7.d-f, while the modeling functions are presented in Fig 7.g-i. Due to the noise and lower concentration in the case of spectrogram and the standard S-method some anomalies may appear in the modeling functions f_1 and f_2. Note that by using the spectrogram, some of the local maxima could be lost as it is the case with points 1, 2 and 3 in Fig 7.h. Thus, f_1 and f_2 are no longer "symmetrical", which leads to the incorrect results.

Similarly, in the case of the standard S-method, the local extremis denoted as 1, 3 and 4 are weak and difficult to detect. Furthermore, $\max(\Delta t)\approx 100$ samples i.e., the distance between local maximum 2 and local minimum 5 is almost 100 samples, which is close to the one arm swinging case (Table II). However, the experiments show that the interferences will be better reduced by the Hermite S-method. Consequently, time-frequency representation is improved in comparison with the spectrogram and the standard S-method. Note that in case of the Hermite S-method, the "symmetrical" structure, typical for the case of both arms swinging, is preserved, with $\max(\Delta t)=22$ samples. The Hermite S-method is less error-prone and hence, more suitable for the classification procedure.

V. Conclusion

A simple but yet effective time-frequency based procedure for classification of radar signals received from human target in motion is proposed. The signatures extracted from the time-frequency domain are used to distinguish between three different types of human walking, namely, human walking without any arm swinging, human walking with one arm swinging, and human walking with both arms swinging. By using the Hermite S-method, a suitable time-frequency representation for radar data analysis is obtained. A good concentration in the time-frequency domain provided easier extraction of the specific motion features and signatures employed in the proposed classifier. The perimeters of the arm micro-Doppler signatures are first captured. The follow up classification procedure, acting on these perimeters, consists of two subroutines: the first one distinguishes between walking with and without arms swinging, while the second renders a classification between one and both arms swinging. The proposed scheme is tested on a set of real radar data collected from different human targets and from two different aspect angles, and shown to provide very desirable classification rates.

REFERENCE

[1] M. Amin and K. Sarabandi (Guest Editors), Special issue on remote sensing of building interior, IEEE Transactions on Geoscience and Remote Sensing, vol. 47, no. 5, May 2009.

[2] M. Amin (Guest Editor), Special issue on Advances in indoor radar imaging, Journal of the Franklin Institute, vol. 345, no. 6, pp. 556–722, Sept. 2008.

[3] D.G. Falconer, K.N. Steadman, and D.G. Watters, "Through-the-wall differential radar," Proc. SPIE Conf. on Command, Control, Communications, and Intelligence Systems for Law Enforcement, Boston, MA, vol. 2938, pp. 147–151, Nov. 1996.

[4] S. Borek, "An overview of through the wall surveillance for homeland security," Proceedings of the 34th Workshop on Applied Imagery and Pattern Recognition, p. 6, Sept. 2005.

[5] A. Hunt, "Image formation through walls using a distributed radar sensor array," Proceedings of the 32nd Applied Imagery Pattern Recognition Workshop, pp. 232 – 237, Sep 2003.

[6] P. Van Dorp and F.C.A. Groen, "Human walking estimation with radar," IEE Proc.- Radar, Sonar, Navigation, Vol. 150, No. 5, October 2003.

[7] V. C. Chen, "Analysis of radar micro-Doppler signature with time-frequency transform," Proc. of the IEEE Workshop on Statistical Signal and Array Processing (SSAP), Pocono, PA, pp.463-466, 2000.

[8] G.E. Smith, K. Woodbridge, and C.J. Baker, "Multistatic micro-Doppler signature of personnel," IEEE Radar Conference, 2008.

[9] L. Cohen, Time-Frequency Analysis, Prentice Hall, 1995.

[10] S. Qian, and D. Chen, Introduction to Joint Time-Frequency Analysis – Methods and Applications, Prentice Hall, Englewood Cliffs, NJ, 1996.

[11] B. Boashash, Time-Frequency Signal Analysis, John Wiley, 1992.

[12] F. Hlawatsch and G.F. Boudreaux-Bartels, "Linear and Quadratic Time-Frequency Signal Representations," IEEE Signal Processing Magazine, pp. 21-67, April 1992.

[13] Time-Frequency Toolbox: http://tftb.nongnu.org/.

[14] B.G. Mobasseri and M. Amin, "A Time-Frequency Classifier for Human Gait Recognition," SPIE Defense, Security and Sensing, vol. 7306, April, 2009.

[15] B. Lyonnet, C. Ioana and M. Amin, "Human Gait Classification using MicroDoppler Time-Frequency Signal Representations," submitted to International Radar Conference, Radar 2010.

[16] Y. Kim and H. Ling, " Human Activity Classification based on MicroDoppler Signatures Using a Support Vector Machine," IEEE Transactions on GeoScience and Remote Sensing, Vol. 47, No. 5, May 2009.

[17] R. Boulic, M. Thalmann, and D. Thalmann, "A global human walking model with real time kinematic personification," Vis. Computer, 6, pp. 334-358.

[18] I. Orović, S. Stanković, T. Thayaparan, and LJ. Stanković, "Multiwindow S-method for Instantaneous Frequency Estimation and its Application in Radar Signal Analysis," IET Signal Processing, accepted for publication

[19] D. N. Kortchagine, A. S. Krylov, "Projection Filtering in image processing," Proc. of the Int. Conf. Graphicon 2000, pp.42-45, 2000.

[20] A. S. Krylov, D. N. Kortchagine, A. S. Lukin, "Streaming Waveform Data Processing by Hermite Expansion for Text-Independent Speaker Indexing from Continuous Speech," Proc. of the Int. Conf. Graphicon 2002, pp. 91-98, Nizhi Novgorod 2002.

[21] S. Stanković, LJ. Stanković, "Introducing Time-Frequency Distribution with a „Complex-lag" Argument," *Eletronic Letters*, vol. 32, No. 14, July 196.

[22] LJ. Stanković, "A method for Time-Frequency Signal Analysis", IEEE *Transaction on Signal Processing*, Vol.42, No.1, January 1994.

[23] LJ. Stanković, V. Ivanović, Z. Petrović, "Unified Approach to the Noise Analysis in the Spectrogram and Wigner distribution," *Annales des Telecommunications*, vol. 51, No. 11/12, pp. 585–594, Nov./Dec. 1996.

[24] G. Frazer, B. Boashash, "Multiple window spectrogram and time-frequency distributions," in *Proc. IEEE ICASSP*, vol. 4, 1994, pp. 193-296.

[25] F. Cakrak, P. J. Loughin, "Multiwindow Time-Varying Spectrum with Instantaneous Bandwidth and Frequency Constraints," IEEE *Transactions on Signal Processing*, vol. 49, No. 8, pp. 1656-1666, August 2001.

[26] M. Bayram, R. G. Baraniuk, "Multiple Window Time-Frequency Analysis," *Proc. of the IEEE Signal Processing International Symposium on Time-Frequency and Time-Scale Analysis*, pp.173-176, Jun 1996.

[27] T. Thayaparan, LJ. Stanković and I. Djurović, "Micro-Doppler Based Target Detection and Feature Extraction in Indoor and Outdoor Environments," *Journal of the Franklin Institute*, vol. 345, No. 6, pp. 700-722, Sept. 2008.